A simplified equivalent circuit model for the study of squeezed film effects in a capacitive MEMS accelerometer

C. KAVITHA*, M. GANESH MADHAN
Department of Electronics Engineering, Madras Institute of Technology, Anna University Chennai, India

A simplified equivalent circuit for the analysis of squeezed film effects in a capacitive MEMS accelerometer is reported in this paper. The reduction of the equivalent circuit is realized by identifying the minimum impedance of the parallel network representing the squeezed film model. The transient and frequency response analysis are carried out in the temperature range of 100K to 400 K, at the pressures of 30Pa, 300Pa and 3000Pa. The results are compared with the experimental and theoretical values reported in literature and the deviations are found to be low as 6% in transient response and less than 5% in the frequency response. It is found that the result of the simplified model agrees well with the detailed model. Due to the circuit reduction, a significant reduction in complexity and computation time is observed.

(Received August 28, 2015; accepted November 28, 2017)

Keywords: Squeezed film damping, Equivalent circuit, MEMS, Capacitive accelerometer, Modeling, Impedance, Dynamic simulation

1. Introduction

MEMS based accelerometers have been widely utilized in recent days. Major applications include automobile airbag triggers, earthquake detection circuits and toys. MEMS accelerometers have advantages over conventional accelerometers due to its small size, light weight, low cost and high reliability [1]. Various MEMS accelerometers have been reported and commercialized; they employ a wide range of detection schemes, including piezoelectric, piezoresistive, capacitive, resonance, optical, magnetic, etc. Capacitive micro machined accelerometers offer several benefits when compared to the piezoresistive or piezoelectric type accelerometers along with good DC response and noise performance. It also posses high sensitivity and low drift [2, 3]. Various capacitive MEMS accelerometers are available commercially, with similar performance, specifications, but with completely different mechanical sensing element designs, materials, packaging and fabrication technologies. The basic structure of a capacitive MEMS accelerometer comprises of a movable micro-beam that responds to accelerations in one or more orthogonal directions. The motion is normally detected as capacitive variation.

In MEMS accelerometers, gas is often employed as a damping medium, which has a significant impact on the accelerometer behavior. The damping of the system is achieved by thin gas films in the gaps between the mass and the fixed electrodes. The compression of gas due to moving plates has to be carefully adjusted to obtain the desired response [4]. Usually the compressible gas films are analyzed using Reynolds equation [5]. This approach has been used by many authors to study the frequency response of micro mechanical pressure sensors [6, 7 and 8]. A number of publications do exit in evaluating squeezed film damping. They include static test, measuring the overshoot and settling time. Finite element methods (FEM) are also employed to study the transient response of the structure [9]. ANSYS, Matlab and analytical model are used to study the different symmetrical beam structures like Z-shaped, H-shaped and Ω-shaped beam capacitive accelerometer [10]. Mathematical models for both open- and closed-loop accelerometers having capacitive sensing and electrostatic feedback have been reported [11]. A structure comprising of two oscillating plates separated by a small gap, is analyzed for the gas viscosity measurements and damping characteristics [7, 8 and 12]. The models were usually viewed as a mass suspended with spring of different structures [13, 14 and 15]. These systems have been conventionally analyzed using finite element and finite difference methods. Circuit representation of mechanical systems is useful, when they are interfaced with electrical systems, for sensing, processing and display of electrical quantities. An equivalent circuit helps to understand the phenomena, and also provides a single platform for the entire analysis.

As MEMS systems include mechanical phenomena and electronic interface, electrical equivalent of the entire system provides the electrical output and also the total response under static and dynamic conditions. A circuit model that involves damping and spring forces created by squeezed film is reported in Ref. [4, 16 and 17]. The equivalent circuit for capacitive MEMS accelerometer, fabricated by Vaisala technologies Inc., is reported and analysis was carried out by comparing the simulated and experimental results [18–20]. Further isothermal compressible squeezed-film damping effects for MEMS devices were reported by Yang et al [21]. The circuit

model of Timo Veijola comprises of linear and nonlinear frequency dependent components to analyze the response of accelerometer under different pressures. They have used a self developed circuit simulation program APLAC [6] for their analysis. This model has been modified to incorporate temperature and pressure variations for PSpice simulation environment [13, 14, 22 and 23]. Timo Veijola has also extended the squeezed film model for perforated structures [24, 25]. This capacitive accelerometer is targeted for developing equivalent circuit model of squeeze film damping. This has applications in personal electronic devices, smart phones, tilt sensor, laptops to protect hard drives from damage, detection of car crashes and deploying airbags, navigation unit, military and aerospace systems.

In this paper, we present a highly simplified electrical equivalent circuit of a low – g capacitive MEMS accelerometers incorporating squeezed film damping. In our approach, the squeezed film effects are implemented using single L-R section, instead of six sections reported in literature [18]. The model is simulated for transient and frequency response, under various pressure and temperature conditions. The circuit is simulated using circuit simulator PSpice. The results are compared with the experimental and detailed equivalent circuit model reported by [4], and found to be in good agreement. The complexities of circuit and computation time are also analyzed. This study also helps to predict the performance of MEMS accelerometer under various viscous mediums and also can be extended to advanced structures. Since the model is based on commercial PSpice simulator, it can be easily integrated with circuit models of other interacting devices and circuits, as most of the device; manufacturer provides SPICE codes for their devices for simulation purpose.

2. Equivalent model for MEMS capacitive Accelerometer

2.1. Cantilever beam displacement model

A simple capacitive accelerometer comprises of a proof mass attached to one end of flexure bar. Two fixed plates are provided one above and another below the flexure bar. The deflection of the flexure bar due to acceleration, results in capacitance variation between the movable and fixed bars. The displacement of flexure bar can be equivalently modeled as a mass- spring- dashpot system as shown in Fig.1. The operation bandwidth depends on the fundamental resonance frequency determined by the mass and the supporting spring.

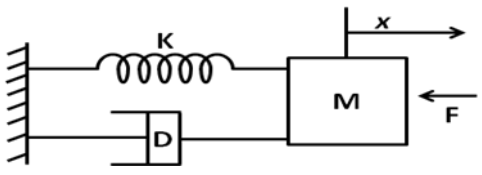

Fig. 1. A generic equivalent of cantilever beam [4]

The mathematical model representing the mass spring dashpot system is given by the following equation.

$$M\frac{d^2x}{dt^2}+D\frac{dx}{dt}+kx=F_{ext}+F_{el} \tag{1}$$

Table 1 Specifications of MEMS capacitive accelerometer [4]

Parameters	Value
Mass M	$4.9\,\mu g$
Width of the moving mass w	$2.96\,mm$
Length of the moving mass l	$1.78\,mm$
Length of the cantilever beam	$520\,\mu m$
Gap widths d_A and d_B	$3.95\pm 0.05\,\mu m$
Mean free path λ at 1 atm	$70.0\pm 0.7\,nm$
Viscosity coefficient η for argon gas	$22.6\pm 0.2\,\mu N.s.m^{-2}$
Temperature T	$100\text{-}400\,K$

where, M , D and k represent the proof mass of the moving plate, damping coefficient and spring constant respectively. The force (F) is the sum of an external mechanical force F_{ext} and an internal electrical attractive force F_{el} . The electrical attractive force on the mass results due to application of potential difference across the capacitor plates, i.e. between flexure bar and fixed plates. Assuming the motion perpendicular to the plate surfaces, the electrostatic force is given as

$$F_{el}=\frac{\varepsilon AU^2}{2d^2} \tag{2}$$

where ε is the dielectric constant of the medium, $A=wl$ is the plate area, U is the capacitor voltage and d is the air gap width of both sides. The mechanical accelerometer model (Eqn.1) is represented by an equivalent electrical model of a parallel resonator and is given by the differential equation as

$$C\frac{d^2\varphi}{dt^2}+\frac{1}{R}\frac{d\varphi}{dt}+\frac{1}{L}\varphi=I_{ext}+I_{el} \tag{3}$$

where C is the capacitance, φ is the flux, R is the resistance, L is the inductance, I_{el} is the electrostatic force current which is created internally and I_{ext} is the external current. The displacement equals, Li_L , where i_L is the current through the inductor. The physical parameters corresponding to a capacitive accelerometer of Vaisala Technologies Inc [4] are shown in Table.1. Timo et al [4] has used the pressures 30Pa, 300Pa, 3000Pa in the temperature range of 22-25°C to analyse squeezed film damping. We have also considered the same pressures in our study for comparison and integrated with temperature effects. The selection of the operating temperature range is based on the requirement for practical MEMS

accelerometers. For example, Analog devices ADXL78, Sherborne Sensors A640 and ST microelectronics AIS1200PS have operating temperature range of 248.15K to 343.15K, 233.15K to 373.15K and 233.15K to 398.15K respectively. Hence, a more elaborate temperature range of 100K to 400K (-173.15°C to 126.85°C) was considered for our study.

2.2. Squeezed film damping model

Damping is provided in order to avoid large displacements, which may otherwise affect the system. Further, damping also improves the dynamic characteristics and increases the bandwidth [26]. In practice, damping is accomplished with the inertial friction of the gas flow in the narrow air gap. The squeezed film damping is modeled using a number of L-R sections connected in parallel. Two such units are used for the corresponding two air gaps. The derivation of L-R sections for squeezed film is provided in detail in Ref. [4]. The expression for L and R components in each section is given by

$$L_{mn} = (mn)^2 \frac{\pi^4 d}{64 A P_a} \tag{4}$$

$$R_{mn} = (mn)^2 (m^2 + c^2 n^2) \frac{\pi^6 d^3}{768 A w^2 \eta_{eff}} \tag{5}$$

where L_{mn} and R_{mn} represent the inductance and resistance model for the squeezed film on air gaps in both sides. m and n are odd integers 1, 3, 5 …, $c = w/l$, while w and l denote the width and length of the proof mass. $\eta_{eff} = \eta / (1 + 9.638(K_n)^{1.159})$ is the effective viscosity, which depends on static pressure (P_a) and viscosity. $\eta = \eta_0 \left(\frac{0.555 T_0 + C}{0.555 T + C} \right) \left(\frac{T}{T_0} \right)^{3/2}$ is the viscosity, dependent on reference viscosity (η_0), temperature (T, T_0) and Sutherland constant (C) of the gas, $K_n = \lambda / d$ is the Knudsen number, $\lambda = P_0 \lambda_0 / P_a$ is the mean free path which is inversely proportional to static pressure P_a, λ_0 is the mean free path at pressure P_0. According to [6], order of sections (n_s) are defined by the following equation

$$m + n \le 2 n_s \tag{6}$$

where, $m = 1, 2, ... n_s$ and $n = 1, 2, ... n_s$. To avoid insignificant component values and to provide good accuracy $n_s = 3$ is considered. The number of sections N can be calculated using the recursive equation as in Ref. [6]

$$N(n_s) = n_s + N(n_s - 1) \tag{7}$$

Hence, six sections are used in the simulations to model both air gaps with odd integers as $(m, n) = (1,1), (1,3), (3,1), (3,3), (1,5), (5,1$. This approach follows the work of [4]. In the proposed work, the numbers of sections (6) in the equivalent circuit are reduced by considering the equivalent impedance of six parallel branches.

2.3. Circuit model of Accelerometer incorporating squeezed film effect

The complete equivalent circuit of the accelerometer comprising of a resonator circuit along with squeezed film model is shown in Fig.2. In resonator circuit, inductance represents the spring element and the resistance accounts for the damping behavior. The accelerometer has two air gaps which are implemented as a two branches connected in parallel, denoted as air gaps A and B. The circuit elements corresponding to the different gaps cannot be combined because the air gap distances are not supposed to be equal. According to equation (4) and (5), the elements L_{mn} and R_{mn} depend on the air gap distance d, area, pressure and viscosity. The values are evaluated and used in the parallel sections of squeezed film model.

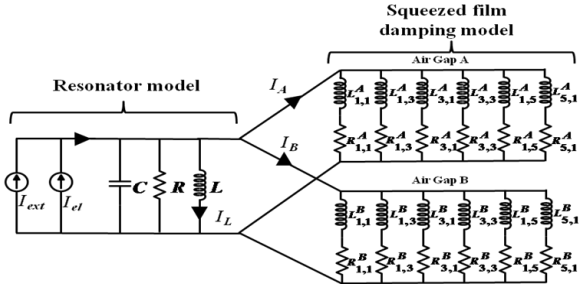

Fig. 2. Full equivalent circuit models with six LR sections for two air gaps [4]

2.3.1. Theory of reduction

Detailed analysis of the six sections model is carried out at various pressures and temperatures. Pressure and temperature dependent variables (Viscosity, Knudsen number, mean free path, Resistance, Inductance) are calculated. The series combination of inductance and resistance is considered as impedance of each section and is represented as $Z_{11} = R_{11} + j(2\pi f L_{11}) = R_{11} + jX_{L11}$. The corresponding reactances and impedances of six sections are evaluated at five different frequencies. For example, at 30Pa and 300K, the reactance and impedance values for the various sections are tabulated in Table 2 and 3 respectively.

Table 2. Magnitude of reactance of each section at different frequencies under 30Pa, 300K

F (Hz)	Reactance					
	$X_{L11}(\Omega)$	$X_{L13}(\Omega)$	$X_{L31}(\Omega)$	$X_{L33}(\Omega)$	$X_{L15}(\Omega)$	$X_{L51}(\Omega)$
1	0.23876	2.14634	2.14634	19.3183	5.96211	5.96211
10	2.3876	21.4634	21.4634	193.183	59.6211	59.6211
100	23.876	214.634	214.634	1931.83	596.211	596.211
1K	238.76	2146.34	2146.34	19318.3	5962.11	5962.11
10K	2387.6	21463.4	21463.4	193183	59621.1	59621.1

Table 3. Impedance of each section at different frequencies under 30Pa, 300K

Impedance in each Section (Ω)	Frequency (Hz)				
	1	**10**	**100**	**1K**	**10K**
Z_{11}	306.59+ j0.23876	306.59+ j2.3876	306.59+ j23.876	306.59+ j238.76	306.59+ j2387.6
Z_{13}	18978.42+ j2.14634	18978.42+ j21.4634	18978.42+ j214.634	18978.42+ j2146.34	18978.42+ j21463.4
Z_{31}	8614.58+ j2.14634	8614.58+ j21.4634	8614.58+ j214.634	8614.58+ j2146.34	8614.58+ j21463.4
Z_{33}	223503.24+ j19.3183	223503.24+ j193.183	223503.24+ j1931.83	223503.24+ j19318.3	223503.24+ j193183
Z_{15}	142824.03+ j5.96211	142824.03+ j59.6211	142824.03+ j596.211	142824.03+ j5962.11	142824.03+ j59621.1
Z_{51}	56458.69+ j5.96211	56458.69+ j59.6211	56458.69+ j596.211	56458.69+ j5962.11	56458.69+ j59621.1
Z_{eff}	289.04687+ j0.21534	289.04742+ j2.15343	289.10193+ j21.5334	294.31007+ j214.28213	429.581051+ j1937.88615

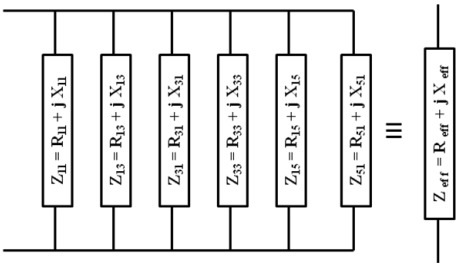

Fig. 3. Six impedance sections connected in parallel

The six LR sections of squeezed film effect are replaced by corresponding impedances and connected in parallel, which is shown in Fig.3. It is well known that in a parallel connection of several impedances, the resultant impedance is almost close to the minimum of impedance in the parallel network. To illustrate this concept, a simple example is considered. Assume two impedances ($Z_{11} = R_{11} + jX_{L11}$ and $Z_{13} = R_{13} + jX_{L13}$) connected in parallel, the equivalent impedance is calculated by

$$Z_{eff} = Z_{11} \|_{el} Z_{13} = \frac{Z_{11}Z_{13}}{Z_{11} + Z_{13}} = R_{eff} + jX_{eff} \qquad (8)$$

If $Z_{11} = 306.59 + j0.23876$ and $Z_{13} = 18978.42 + j2.14634$ then $Z_{eff} = 301.71588 + j0.23177$. This value is close to $Z_{11} = 306.59 + j0.23876$. Similarly the equivalent impedance (Z_{eff}) is identified for six impedances connected in parallel. In the case of 30Pa, 300K, the equivalent impedance (Z_{eff}) of the parallel combination is 289.04687+jf0.21534Ω. This value is very close to Z_{11} impedance value, i.e. 306.59+jf0.23876Ω. It is found that, among the six parallel sections in air gap A or B, the section offering the minimum impedance value will dictate the overall circuit behavior. Hence, we attempt to simplify the model by replacing the six LR sections by a single LR section, which provides the minimum impedance. However a slight difference arises between the lowest impedance in the network and the actual equivalent impedance. The actual equivalent impedance (Z_{eff}) of the parallel connection is calculated and provided in the last row of Table 3. This effect will be analyzed in the subsequent sections. From the calculation and Table 3, it is found that the minimum impedance is offered by the section corresponding to $(m, n) = (1,1)$. This section alone is used for the proposed model and the reduced expressions for L_{11}, R_{11} (eqn.4 &5) are given by

$$L_{11} = \frac{\pi^4 d}{64 A P_a} \tag{9}$$

$$R_{11} = (1+c^2)\frac{\pi^6 d^3}{768 A w^2 \eta_{eff}} \tag{10}$$

The effect of the difference on the performance is determined by simulation. The simplified circuit with single LR section for top and bottom air gaps is shown in Fig.4.

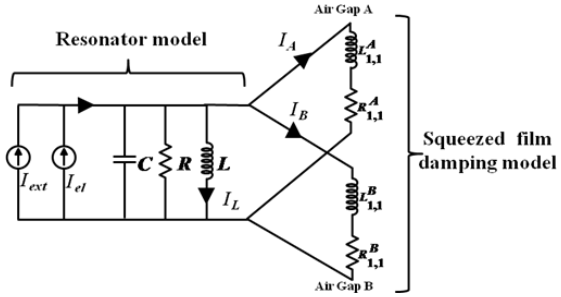

Fig. 4. Simplified equivalent circuit

Single axis capacitive accelerometer is used to measure acceleration only along one axis. To obtain accelerations in three axis, the model has to be modified to include force-equivalent currents in three axis and three parallel branches of resonator circuits are required to provide displacement along three axis separately. The signal conditioning circuit includes a buffer amplifier, a filter, a synchronous demodulator and electro-mechanical feedback loop with a feedback amplifier. The signal conditioning circuit reads the signal from the capacitive accelerometer.

3. Simulation results

In order to validate our approach, simulations have been carried out using PSpice circuit simulator, for both six sections and simplified single section models. Various pressures and temperatures have been considered, as they influence the squeezed film characteristics predominantly. Further the reduction in circuit complexity and computation time are also determined.

3.1. Transient response

Evaluation of transient response is carried out by providing a step input acceleration of 0.5g, which is represented equivalently as a 24.0345μA current pulse in the equivalent circuit [4]. The displacement of the flexure bar is determined, at a temperature and pressure of 100K and 30 Pa respectively. Under this condition, the displacement is characterized by large oscillations, as shown in Fig.5.

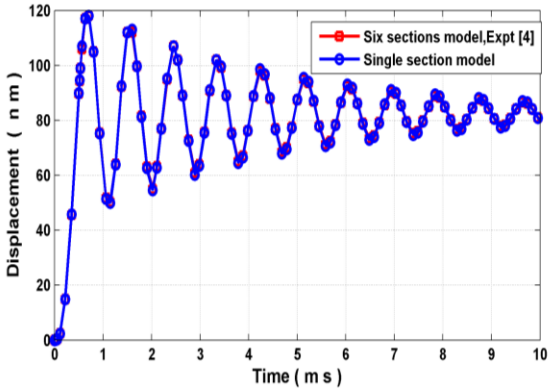

Fig. 5. Transient response analysis under 100K, 30Pa

It is observed that the results obtained using six sections model and single section model exactly matches with each other. Simulations repeated for 100K and 300 Pa, also shows good matching, thereby validating our proposed concept. Further, the displacement is found to reach steady state at short time, with increased damping. This behavior is illustrated in Fig. 6. At 3000 Pa, the damping is highly pronounced and the corresponding response is shown in Fig. 7. It is evident that higher pressures lead to significant damping. Further, an increase in rise time with pressure is also noted. The analysis is repeated for different temperatures. It is found that, higher temperatures lead to reduced displacement amplitude. In this analysis also, the results obtained for six sections, experimental and our proposed single section model agree well.

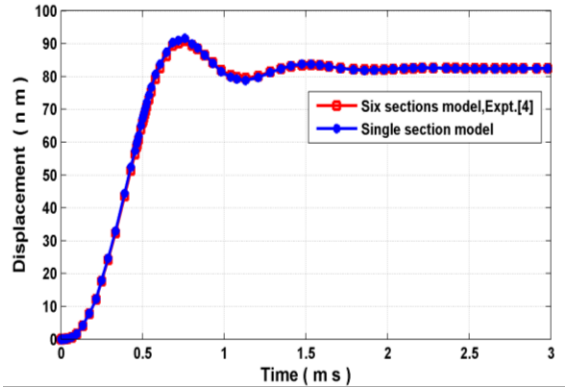

Fig. 6. Transient response analysis under 100K, 300Pa

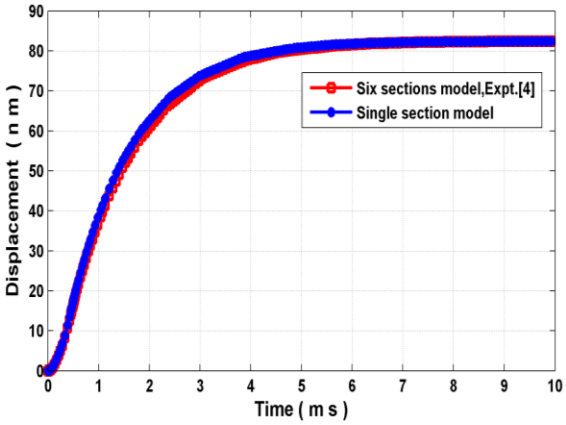

Fig. 7. Transient response analysis under 100K, 3000Pa

In order to validate our approach, we consider two different magnitude of external forces viz. 96.138μA, 144μA corresponding to an acceleration of 2g, 3g respectively. At 100K temperature and 30Pa pressure, the transient response analysis is performed and the results are shown in Fig.8. and Fig.9. This shows the comparison between six sections model and single section model and the experimental results [4]. It proves the proportional relation between acceleration and amplitude.

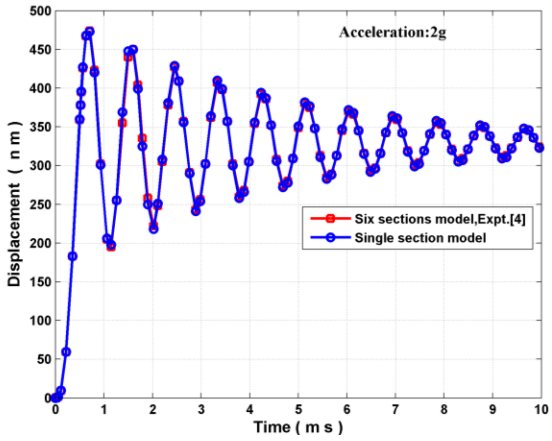

Fig. 8. Transient response analysis under 100K, 30Pa at acceleration of 2g

The rise time and settling time for the two models are calculated for the different pressures at a constant temperature of 100K and shown in Fig.10 and Fig.11 respectively. The rise time is found to increase with gas pressure. In the case of settling time, it decreases with increasing pressure till 600Pa and increases beyond that. For both rise time and settling time analysis, the six section model and single section model provide close results for the input acceleration of 0.5g.

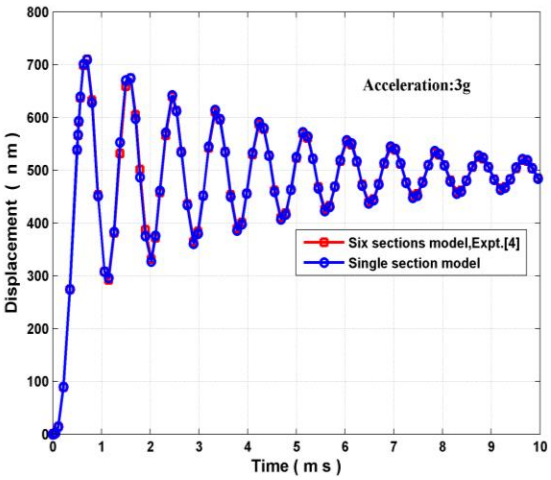

Fig. 9. Transient response analysis under 100K, 30Pa at acceleration of 3g

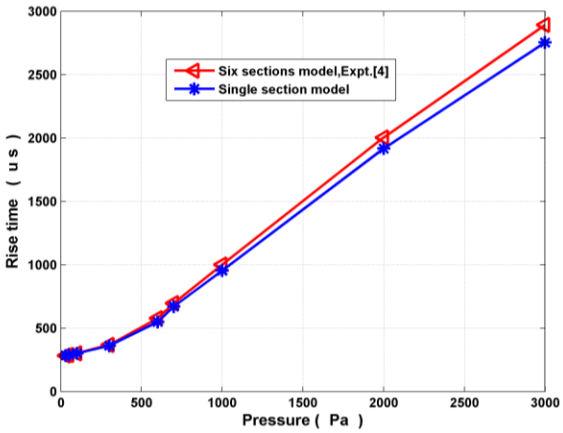

Fig. 10. Pressure versus Rise time for both models

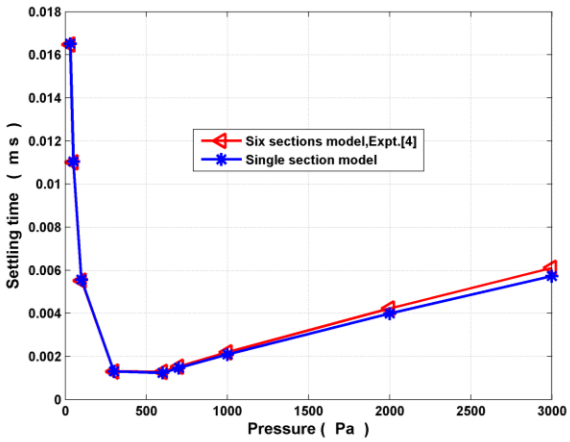

Fig. 11. Pressure versus settling time for both models

3.2. Frequency response

For this simulation, acceleration is represented as 24.0345 μA sinusoidal current which is applied externally to the circuit. The displacement is measured for a range of frequencies at different operating pressures. For example, in the case of 100K, 30 Pa, the resonant frequency is observed at 1.2589 KHz. The frequency responses are shown in Fig.12 and 13. The resonant frequency in the case of 300 Pa is also found to be equal to 1.2589 KHz. Comparison with proposed single section model shows good agreement. But for higher pressures of 1500Pa and 3000Pa, the resonance frequency shifts to 3.5 KHz and 5 KHz respectively. Further, a slight deviation in the response of the proposed model and the six section model, around resonance, is observed and is shown in Fig.14 and Fig.15.

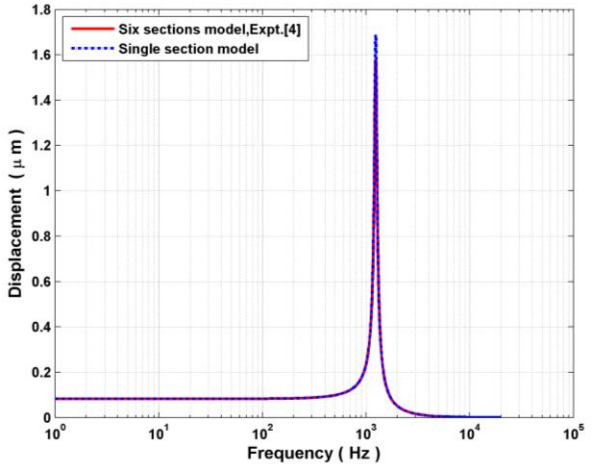

Fig. 12. Frequency response analysis under 100K, 30Pa

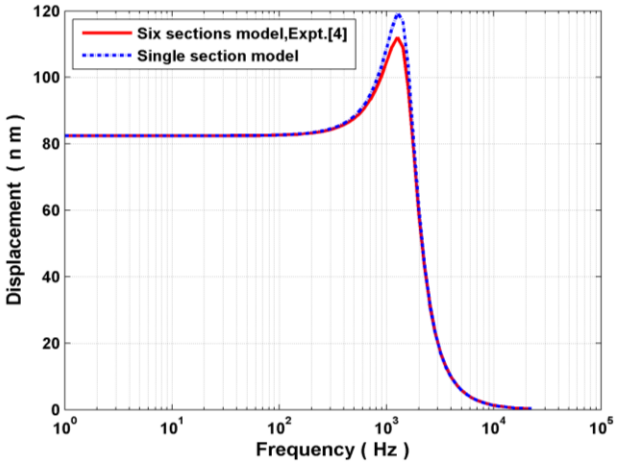

Fig. 13. Frequency response analysis under 100K, 300Pa

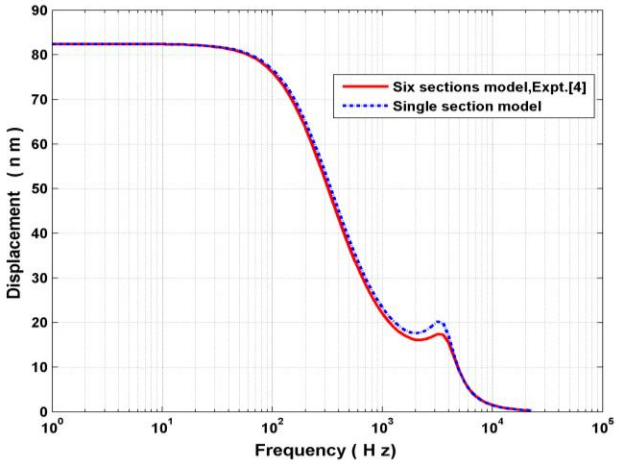

Fig. 14. Frequency response analysis under 100K, 1500Pa

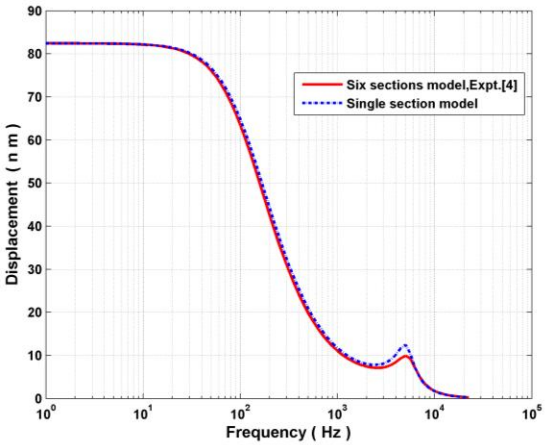

Fig. 15. Frequency response analysis under 100K, 3000Pa

The peak amplitude of displacement at resonance frequency is reduced by increasing the gas pressure. This is due to the fact that viscosity losses are larger than the energy storage effect of the squeeze film under compression. A flat frequency response is obtained below resonance frequency which is the normal operating range of the device.

In order to compare the results, we consider different magnitude of external forces viz. 96.138μA, 144μA corresponding to 2g, 3g acceleration respectively. Frequency response analysis is carried out under 100K temperature and 30Pa pressure condition and the results are shown in Fig. 16 and Fig.17. With respect to increase in acceleration, amplitude of peak displacement also increases. The comparison between six sections model and single section model and the experiment [4] produces exactly similar results, thereby validating our methodology. All literatures report that, squeezed film damping reduces overshoot and minimize the resonant peak. In our analysis also, we have obtained similar results. This proves our modeling approach.

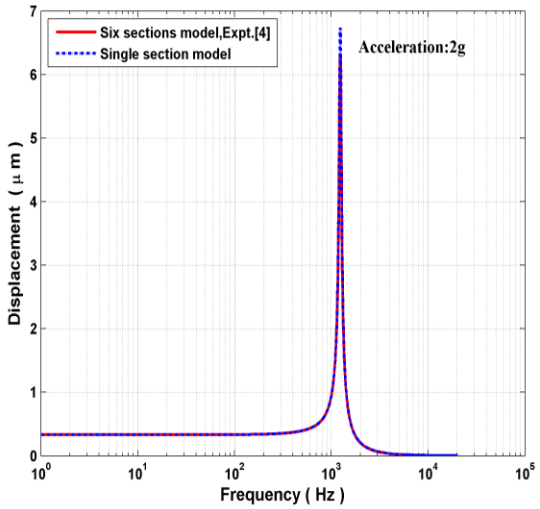

Fig. 16. Frequency response analysis under 100K, 30Pa at acceleration of 2g

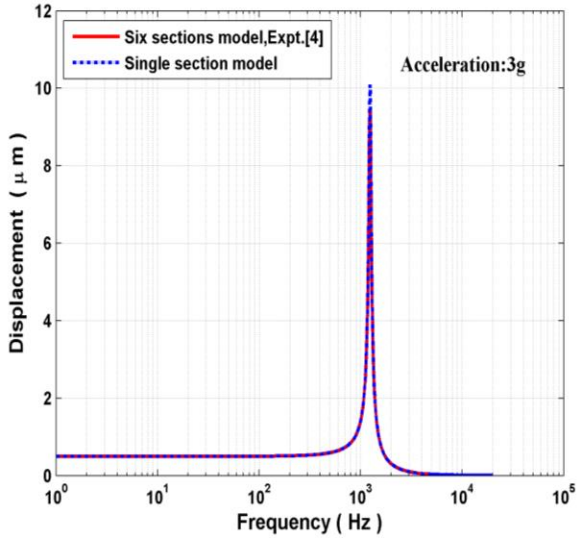

Fig. 17. Frequency response analysis under 100K, 30Pa at acceleration of 3g

3.3. Percentage error calculation

In order to examine the deviation of the response between the two models, an elaborate error calculation is carried out for both transient and frequency response analysis. It is computed by considering the maximum deviation from the six sections model. It is observed that the maximum error in transient condition is less than 6% only. In the case of frequency response, a slight deviation is obtained only at resonance frequency. However, the error percentage is less than 5% in all other frequencies except resonance. As the device is conventionally operated far below resonant frequency [4] and at lower pressures [27, 28 and 29], this error need not be considered seriously. Further, literature reports indicate as the vibration components are measured by error no more than +12% [30], the deviation is acceptable. The percentage of error is calculated using the numerical formulae

$$\% \, Error = \frac{ABS(Single\ Section\ Value - Six\ Sections\ Value)}{Six\ Sections\ Value} \times 100 \quad (11)$$

Here, the single section value is calculated from our proposed model and six sections model value is evaluated from the detailed scheme [4].

Table 4. Computation time between two models

Execution time for computing displacement (Seconds)							
Response	T (K)	Six sections model			Single section model		
		30Pa	300Pa	3000Pa	30Pa	300Pa	3000Pa
DC	100	0.73	0.44	0.41	0.44	0.22	0.14
	200	0.69	0.39	0.34	0.36	0.23	0.2
	280	0.61	0.39	0.42	0.38	0.27	0.19
	300	0.69	0.39	0.34	0.45	0.25	0.19
	400	0.69	0.39	0.33	0.33	0.27	0.2
AC	100	0.78	0.44	0.39	0.44	0.22	0.19
	200	0.69	0.47	0.33	0.36	0.22	0.19
	280	0.67	0.41	0.34	0.38	0.27	0.17
	300	0.63	0.38	0.38	0.42	0.3	0.19
	400	0.66	0.38	0.42	0.41	0.3	0.22
Transient	100	0.75	0.44	0.41	0.42	0.19	0.19
	200	0.64	0.31	0.33	0.38	0.28	0.19
	280	0.72	0.41	0.38	0.39	0.25	0.19
	300	0.7	0.49	0.38	0.38	0.28	0.22
	400	0.63	0.42	0.38	0.44	0.31	0.19

Table 5. Average of Computation Time

Average of computation time (Seconds)						
Analysis	Six sections model			Single section model		
	30 Pa	300 Pa	3000 Pa	30 Pa	300 Pa	3000 Pa
DC	0.682	0.4	0.368	0.392	0.248	0.184
AC	0.686	0.416	0.372	0.402	0.262	0.192
Transient	0.688	0.414	0.376	0.402	0.262	0.196

3.4. Computation time and Complexity

The circuit implementation of the proposed model has resulted in 9 nodes, whereas the six section scheme required 19 nodes in a standard PSpice implementation. The circuit simulated using a 3.10 GHz, Intel core i5 processor with 3 GB RAM resulted in significant reduction of computation time. The execution time for computing displacement as reported by the output file of the PSpice Version 10.3 simulator is in "seconds". This computation time is taken for the analysis and given in Table.4.

The computation time between six section and single section is obtained as an average reduction of 29%, 15% and 18% at DC, AC and transient response respectively. It is concluded that, on an average, around 20% reduction is found in the computation time between two models. The average reduction of computation time between two models is calculated and is given in Table.5. as follows

$$\%Reduction\ of\ Computation\ Time = \left(\frac{Single\ Section\ Computation\ Time}{Six\ Section\ Computation\ Time} \right) \times 100 \quad (12)$$

The average of percentage computation time is calculated under different temperatures for 30Pa, 300Pa and 3000Pa respectively at DC, AC and Transient characteristics is shown in Table.6.

Table 6 Average of percentage reduction of computation time at DC, AC and Transient analysis

Pressures (Pa)			
Analysis	30	300	3000
DC (%)	57.56	62.31	51
AC (%)	58.82	64.11	51.73
Transient (%)	58.73	65.09	52.36

The obtained percentage reduction of computation time is 58%, 64% and 52% for 30Pa, 300Pa and 3000Pa respectively at DC, AC and Transient characteristics. 10 nodes are less in single section model compared to six sections model. It is inferred that around 50% reduction in complexity occurs in our proposed model. For the present day workstations, it may be quite an easy task. However, for detailed modeling of the complete MEMS accelerometer chip, which comprises of an equivalent circuit for mechanical systems, electronic circuits for interfacing and further processing, power supply circuit, etc., reduction in number of nodes become significant. Further, the model is developed in PSpice, which is compatible with majority of the IC manufacturer's design.

4. Conclusions

A simplified SPICE model for analyzing squeezed film effects is reported in this paper. Comparison of the results obtained by simulating the six section model and experiment of (Timo Veijola et al., 1995) and our proposed model, under similar operating platform, reveals a deviation of 6% only, at transient analysis. In the case of frequency response analysis, a slight deviation is observed, around resonance frequency. Since the device is normally operated at frequencies far below resonance, the variations due to simplified model is not significant. However, in all other frequency ranges the error is less than 5%. Advantages of our proposed model include 50% reduction in computation time and reduced complexity, which might be important in simulation of entire circuit including mechanical accelerometer model.

References

[1] F. Mohd-Yasin, D. J. Nagel, D. S. Ong, C. E. Korman, H. T. Chuah, Microelectron. Eng. **84**, 1788 (2007).

[2] N. Barbour, G. Schmidt, IEEE Sens. J. **1**, 332 (2001).

[3] N. Yazdi, F. Ayazi, K.. Najafi, Proc. IEEE. **86**, 1640 (1998).

[4] Timo Veijola, Heikki Kuisma, Juha Lahdenperä, Tapani Ryhänen, Sensor Actuat. A-Phys. **48**, 239 (1995).

[5] W. A Gross, Gas Film Lubrication, Wiley, New York, NY (1962).

[6] T. Veijola, Accelerometer model in APLAC, Technical Report CT-18. TKK offset, Espoo (1994).

[7] M. K.. Andrews, G. C. Turner, P. D. Harris, I. M. Harris, Sensor Actuat. A-Phys. **36**, 219 (1993).

[8] M. Andrews, I. Harris, G. Turner, Sensor. Actuat. A-Phys. **36**, 78 (1993).

[9] Y.M. Mo, L.M. Du, B.B. Qu, B. Peng, J. Yang, Wireless Sensor Network **9**, 178 (2017).

[10] Keya Sanyal, Kalyan Biswas, Devices for Integrated Circuit (DevIC), 2017, p. 294.

[11] C. P. Lewis, M. Kraft, T. G. Hesketh, T. I. Meas. Control **18**, 92 (1996).

[12] M. K. Andrews, P. D. Harris, Sensor. Actuat. A-Phys. **49**, 103 (1995).

[13] C. Kavitha, M. Ganesh Madhan, Procedia Eng. **64**, 292 (2013).

[14] C. Kavitha, M. Ganesh Madhan, J. Nano- Electron. Phys. **5**, 02011(2013).

[15] Cenk Acar, Andrei M Shkel, J. Micromech. Microeng. **13**, 634 (2003).

[16] Timo Veijola, Heikki Kuisma, Juha Lahdenperä, Proc. Intern. Conf. Modeling and Simulation of Microsystems (MSM'98), 1998, p.245.

[17] T. Veijola, Equivalent Circuit models for Micromechanical Inertial Sensors, Technical Report CT-39, HUT, Espoo (1999).

[18] Timo Veijola, J. Micromech. Microeng. **14**, 1109 (2004).

[19] T. Veijola, Proc. Sensors, 2007, p.83.
[20] T. Veijola, H. Kuisma, J. Lahdenpera, Proc. Transducers'97, Intern. conf. on Solid State Sensors and Actuators **2**, 1097 (1997).
[21] Y. J. Yang, S. D. Senturia, Technical Digest, IEEE Solid State Sensor and Actuator workshop, 1996, p.76.
[22] C. Kavitha, M. Ganesh Madhan, J. Braz. Soc. Mech. Sci. Eng. **38**, 241 (2016).
[23] C. Kavitha, M. Ganesh Madhan, J. Braz. Soc. Mech. Sci. Eng. **39**, 925 (2017).
[24] Timo Veijola, Microfluid. Nanofluid. **6**, 203 (2009).
[25] T. Veijola, Proc. Design, Test, Integration and Packaging of MEMS/MOMEMS (DTIP 2009), 2009, p.243.
[26] L. Xiaowei, C. Hong, C. Weiping, 6-th Intern. Conf. on Electronic Packaging Technology (ICEPT), 2005, p.1.
[27] Haifeng Lv, Chengyu Jiang, Zhijie Xiang, Binghe Ma, Jinjun Deng, Weizheng Yuan, Flow. Meas. Instrum. **30**, 65 (2013).
[28] Stanisław Kaliciński, Tomasz Bieniek, Paweł Janus, Piotr Grabiec, Microelectron. Reliab. **51**, 1192 (2011).
[29] L. Mol, L. A. Rocha, E. Cretu, R. F. Wolffenbuttel, J. Micromech. Microeng. **19**, 074021 (2009).
[30] https://www.bksv.com/media/doc/br0094.pdf

*Corresponding author: kaviphd2011@yahoo.co.in, mganesh@annauniv.edu